BeBeC-2014-12

A THEORETICAL AND EXPERIMENTAL COMPARISON OF THE ITERATIVE EQUIVALENT SOURCE METHOD AND THE GENERALIZED INVERSE BEAMFORMING

B. Oudompheng[1,3], A. Pereira[2], C. Picard[1], Q. Leclère[2] and B. Nicolas[3]
[1]MicrodB
28 Chemin du Petit Bois, 69134, Écully, France
benoit.oudompheng@microdb.fr
[2]Laboratoire Vibrations Acoustique, INSA Lyon
25 bis Avenue Jean Capelle, 69621, Villeurbanne Cedex, France
[3]GIPSA-Lab
11 Rue des Mathématiques, 38402, Saint-Martin d'Hères Cedex, France

ABSTRACT

Many acoustic source mapping methods exist to perform noise source localization and quantification and appear to be powerful tools for acoustic diagnosis in industrial applications. Two classes of methods have known many developments in the last few decades: deconvolution algorithms combined with beamforming (CLEAN, DAMAS, etc) and inverse methods such as the Equivalent Source Method (ESM) and the Generalized Inverse Beamforming (GIB). In this paper, a special attention will be paid to the use of inverse methods in complex acoustic environments. Recently, Suzuki has demonstrated the applicability of the GIB to the study of aerodynamic sound sources [25], highlighting comparable performances to the existing deconvolution techniques. On the other hand, an iterative version of the ESM has been proposed in the context of acoustic imaging in closed spaces, at INSA Lyon [22].
This paper provides a theoretical and experimental comparison between two inverse methods: the iterative ESM and the GIB using various benchmark problems and aeroacoustic experimental data. The experimental set-up consists of a steel rod placed in the potential core of a rectangular jet inside an open-jet anechoic wind tunnel. It will be shown that both methods are based on similar mathematical formulations although they were developed for different application fields. Reconstruction performances of the algorithms in terms of localization and quantification will be discussed as well as their computational efficiency.

1 INTRODUCTION

Improving localization and quantification in complex acoustic environments has become a current challenge for the acoustic source identification community because of the complex nature of the sources (aeroacoustic sources) and the uncertainties about the propagation medium (reverberation, refraction). In these days, source identification methods are Near-Field Acoustical Holography [20], Beamforming based methods: deconvolution methods of Beamforming results (DAMAS [2], CLEAN-SC [23]), advanced time-domain Beamforming techniques [7], robust Capon [6, 18]. Few inverse methods requiring mathematical inversion of the transfer matrix have been developed and demonstrated as feasible to deal with complex acoustic imaging issues, due to the strong sensitivity of inverse methods to modelling errors and measurement noise. Recently, Suzuki proposed the Generalized Inverse Beamforming (GIB) which considers the source identification inverse problem as a L_1 norm problem and which models the source distribution as a linear combination of monopole sources and dipole sources. Many experimental results have confirmed its applicability to aeroacoustic source mapping (laboratory experiments [27], jet noise [8], jet-flap interaction noise [25]). In context of acoustic measurements in enclosed spaces, Pereira developed an iterative version of the Equivalent Source Method (iESM) during his thesis [22] based on an iterative resolution of the acoustic inverse problem in the least square sense. Our interest in this paper is to provide a theoretical and an experimental comparison between GIB and the iESM in order to discuss the differences of these so close algorithms. Indeed, even though the two methods were developed in two different fields of acoustics, they share a common mathematical formulation. They use an iterative scheme to compute an efficient source reconstruction in complex acoustic environment, both in terms of localization and quantification of acoustic sources. Inverse methods such as GIB and iESM have the benefit to simultaneously backpropagate the measured acoustic energy to every grid points, these grid points are called equivalent acoustic sources and describe the acoustic radiation of an acoustic radiating object. Thus, the proof of their feasibility in aeroacoustics will provide an alternative to deconvolution Beamforming based algorithms whose physical interpretation still remains uncertain.
The paper is organized as follows. Section 2 presents the algorithms of both methods and compares them through mathematical aspects. Section 3 compares the source reconstruction performances of the methods for benchmark problems described by Suzuki in [25]. Section 4 examines the practical capabilities of the methods with the experimental set-up of a rod in the potential core of a rectangular jet inside an open-jet anechoic wind tunnel. Section 5 finally gives some conclusions and perspectives for the use of inverse methods for aeroacoustic source identification.

2 OUTLINE OF THEORY

2.1 Formulation of the acoustic source identification problem

The GIB method and the iESM method consider a discretized version of the direct acoustic problem. Assuming that it is possible to define a virtual acoustic source distribution which radiates the same acoustic field as the real sources, this distribution can be discretized in N equivalent acoustic sources. Generally speaking, the equivalent sources are elementary sources which represent a likely complex structure, the parameters of equivalent sources being deter-

mined such that they match some prescribed or measured data. This principle is at the basis of the Equivalent Source Method (ESM), or wave superposition method, which was introduced to the acoustical community by Koopmann *et al.* [16]. It was initially applied to acoustic radiation problems from arbitrarily shaped sources, a historical overview of ESM and its variants in acoustics may be found in [19]. Given M measuring points of a microphone array and assuming a free-field propagation, the direct acoustic problem is expressed by the following linear system, using a matrix notation:

$$\mathbf{p} = \mathbf{G}\mathbf{q} + \mathbf{n}, \tag{1}$$

where $\mathbf{p}$ is a $M \times 1$ vector of complex measured acoustic pressure, $\mathbf{q}$ the volume velocity of $N \times N_{type}$ *unknown* equivalent sources, $\mathbf{n}$ accounts for the $M \times 1$ vector of measurement noise and $\mathbf{G}$ is a $M \times (N \times N_{type})$ matrix of Green's functions. N_{type} is the number of multipole types considered for the description of each equivalent sources. We precise that the complex vector $\mathbf{p}$ may represent, for instance, a spectrum vector as returned from an eigen decomposition of the cross-spectral matrix, a snapshot of a Short Time Fourier transform (STFT) of pressure signals or eventually the complex pressure vector estimated using a reference sensor.

In practice, the number of equivalent sources used for representing the source is usually higher than the number of available measurements, i.e., $M < N \times N_{type}$. This leads to an underdetermined and ill-posed problem, in the sense that it has an infinite number of solutions and the solution is not stable with respect to, even small, uncertainties on the measured data. Additional *a priori* information is thus required in order to find physically meaningful solutions. This information could, for instance, be related to the energy of the solution (e.g. Tikhonov regularization [26]), to its sparsity at the reconstruction basis or at some other representation basis [3, 5, 21].

2.2 Generalized Inverse Beamforming (GIB)

Let the estimated cross spectral matrix of the measured acoustic pressures $\mathbf{p}$ be noted Λ, it is square and hermitian so its orthogonal decomposition can be carried out by an eigenvalue decomposition:

$$\Lambda = \mathrm{E}[\mathbf{p}\mathbf{p}^H] = \mathbf{U}_\Lambda \Sigma_\Lambda \mathbf{U}_\Lambda^H \tag{2}$$

where $\mathbf{U}_\Lambda$ is the unitary eigenvector matrix of Λ of dimension $M \times M$ and Σ_Λ the eigenvalue diagonal matrix. From this decomposition, the M eigenmodes are defined as:

$$\text{For } m \in [1, M], \qquad \mathbf{p}_m = \sqrt{\sigma_m}\mathbf{u}_m \tag{3}$$

where $\mathbf{p}_m$ is a $M \times 1$ vector, σ_m is the m^{th} greatest eigenvalue of Λ and $\mathbf{u}_m$ the column of $\mathbf{U}_\Lambda$ related to σ_m. $\mathbf{u}_m$ is an eigenvector of Λ and represents a set of coherent signals, two distinct eigenvectors are orthogonal.

The goal of GIB algorithm is to find the source distribution that recovers each eigenmode which is consistent to an acoustic pressure signal. In order to identify the source distribution corresponding to an eigenmode, an inverse problem is formulated introducing the transfer matrix $\mathbf{G}$ linking the calculation grid (the set of equivalent sources) to the microphone array:

$$\text{For } m \in [1, M], \qquad \mathbf{p}_m = \mathbf{G}\mathbf{q}_m \tag{4}$$

where $\mathbf{q}_m$ is the complex equivalent source amplitude vector of dimension $N \times N_{type} \times 1$, related to the m^{th} eigenmode . In this study, monopole equivalent sources and two types of dipole equivalent sources will be considered, $N_{type} = 3$. The two types of dipole equivalent sources are dipole sources in the x direction and dipole sources in the y direction. At this step of the algorithm, it is important to point out that the set of coherent signals corresponding to a mode of the cross spectral matrix does not refer to a set of physical sources but to a set of virtual sources which satisfy a property of orthogonality. As a result, the source distributions $\mathbf{q}_m$ equivalent to the most energetic modes of the cross spectral matrix should be summed in energy to represent the global system.

Least square inverse solution tends to provide smooth and blur acoustic source maps in terms of localization whereas most sources are compact. To improve the resolution and to recover the compactness of reconstructed sources, Suzuki proposes to use a penalization factor on the $L_p, 0 \leq p \leq 1$ norm of the target solution of the inverse problem. The L_p-minimization problem can be formulated as:

$$\text{minimize} \quad \left\{ \|\mathbf{p}_m - \mathbf{G}\mathbf{q}_m\|_2^2 + \eta^2 \|\mathbf{q}_m\|_p^p \right\}, \tag{5}$$

$L_p, 0 \leq p \leq 1$ norm choice is made to enhance the sparsity of the target solution of the inverse problem, i.e. it minimizes the number of equivalent sources with non zero amplitude. In the whole article, $p = 1$ is considered because it ensures the convexity of the minimization problem, i.e. the existence of a unique optimal solution. To solve this L_1-norm inverse problem, Suzuki first proposed a Newton-Raphson algorithm [24] which sometimes gives unstable results (irrelevant estimated source amplitude, etc). More recently, the IRLS algorithm (Iteratively Reweighted Least Squares [14]) has been preferred for its more stable results [25], it consists of computing the least square solution and introducing a weighting matrix $\mathbf{W}$ at each iteration. At the n^{th} iteration of the algorithm, for the m^{th} eigenmode, the weighting matrix is equal to the equivalent source amplitudes $\hat{q}_{i,m}^{(n-1)}, i \in [1, N \times N_{type}]$ which were estimated at the previous iteration:

$$\text{For } (i,j) \in [1, N \times N_{type}] \times [1, N \times N_{type}], \qquad W_{ij,m}^{(n)} = \delta_{ij} |\hat{q}_{i,m}^{(n-1)}| \tag{6}$$

where δ_{ij} is the Kronecker symbol. The solution of Eq. (5) with respect to IRLS algorithm can be expressed as:

$$\text{For } m \in [1, M], \qquad \hat{\mathbf{q}}_m^{(n)} = \mathbf{W}_m^{(n)} \mathbf{G}^H \left[\mathbf{G}\mathbf{W}_m^{(n)} \mathbf{G}^H + \eta^2 \mathbf{I} \right]^{-1} \mathbf{p}_m \tag{7}$$

In Suzuki's version of GIB, the regularization parameter η^2 is determined by a diagonal loading technique similarly to the methodologies employed in Capon algorithms [6] [18]. Here, the regularization parameter η^2 is arbitrarily chosen equal to 1% of the greatest eigenvalue of $\mathbf{G}\mathbf{W}_m^{(n)}\mathbf{G}^H$. To save computational time, at the n^{th} iteration of the algorithm, only the $\beta^n \times N \times N_{type}$ estimated equivalent sources with the greatest amplitude modulus are used for the next iteration.

As mentioned above, the estimated source amplitude vector $\mathbf{q}_m$ related to each eigenmode $\mathbf{p}_m$ and to the greatest eigenvalues σ_m are summed in order to get an estimate of the whole source distribution:

$$\mathbf{q} = \sum_m \mathbf{q}_m \tag{8}$$

Two stopping criteria are defined to end the algorithm. The first criterion indicates the convergence of the algorithm, it consists of stopping the iteration process when the L_1 norm of the equivalent source amplitude vector has increased from an iteration to the next one. It is written as:

$$\sum_{i=1}^{N} |\mathbf{q}_{i,m}^{(n)}| = \|\hat{\mathbf{q}}_m^{(n)}\|_1 > \|\hat{\mathbf{q}}_m^{(n-1)}\|_1 \tag{9}$$

The second stopping criterion concerns the minimum number of equivalent sources. Indeed, as mentioned above, at each iteration, only the equivalent sources with the highest amplitudes are used for the next iteration. In this study, the iteration process ends when the following condition is met at the n^{th} iteration:

$$2M > \beta^n \times N \times N_{type} \tag{10}$$

This criterion means that the implementation of the GIB is here restricted to underdetermined cases, i.e. $M < \beta^n \times N \times N_{type}$ at the n^{th} iteration. Suzuki suggests the possibility to solve the overdetermined cases [25], when $\beta^n \times N \times N_{type} < M$, in order to let the iteration process converge and meet the first stopping criterion. Benchmark cases of section 3 and experimental data presented in section 4 have been processed by GIB by accounting for overdetermined cases but it has not improved physical interpretation of the results. Consequently, the choice was made to limit this study to underdetermined problems. Moreover, satisfying Eq. (10) also is a means to keep a sufficient number of equivalent acoustic sources in order to reduce the sparsity of the results, thus a means to hope a better physical interpretation.

2.3 Iterative Equivalent Source Method (iESM)

In a least square sense, the resolution of the problem in Eq. (1) consists of the minimization of a residual error (between measured and reconstructed pressure) plus an additional constraint on the energy of the solution:

$$\text{minimize} \quad \left\{ \|\mathbf{p} - \mathbf{G}\mathbf{q}\|_2^2 + \eta^2 \|\mathbf{q}\|_2^2 \right\} \tag{11}$$

The solution of this least square problem can be expressed using the generalized inverse because the transfer matrix is rectangular:

$$\hat{\mathbf{q}} = \mathbf{G}^{\dagger}\mathbf{p} \tag{12}$$

where $\bullet^{\dagger}$ denotes the Moore-Penrose pseudo-inverse. In most acoustic studies, the number of microphones is limited which implies that the inverse problem Eq. (4) often is underdetermined: the number of grid points is higher than the number of measuring points, i.e. $M < N \times N_{type}$, and the transfer matrix is ill-conditioned. The algorithm is implemented with monopole transfer functions so $N_{type} = 1$. An underdetermined problem does not have a unique solution so a regularization technique is required to find the optimal solution of Eq. (4). In acoustics, the Tikhonov regularization is generally used [26]:

$$\hat{\mathbf{q}} = \mathbf{G}^H \left[\mathbf{G}\mathbf{G}^H + \eta^2 \mathbf{I} \right]^{-1} \mathbf{p} \tag{13}$$

Inspired on the application of the ESM for acoustic imaging purposes within a closed space, additional information on the problem was introduced in the form of a weighting matrix [22]. The motivation was to correct for the positioning of the acoustic microphone array inside the

enclosure, such that those equivalent sources which are closer to the array are not favored on the minimization. In that context, the weighting was related to the distance between each equivalent source and the center of the array. The introduction of the above *a priori* information leads to the following minimization problem:

$$\text{minimize} \quad \left\{ \|\mathbf{p} - \mathbf{G}\mathbf{q}\|_2^2 + \eta^2 \|\mathbf{W}\mathbf{q}\|_2^2 \right\}, \tag{14}$$

with the square diagonal matrix $\mathbf{W}$ of dimensions $N \times N$. The above problem is recognized as the general form of Tikhonov regularization in the literature [11]. If $\mathbf{W}$ is invertible such that $\mathbf{W}\mathbf{W}^{-1} = \mathbf{I}$, which is the case for any diagonal matrix with non-zero diagonal entries, we can modify the above minimization problem by introducing the transformation $\mathbf{q} = \mathbf{W}^{-1}\tilde{\mathbf{q}}$ and thus arrive at the following minimization problem:

$$\text{minimize} \quad \left\{ \|\mathbf{p} - \mathbf{G}\mathbf{W}^{-1}\tilde{\mathbf{q}}\|_2^2 + \eta^2 \|\tilde{\mathbf{q}}\|_2^2 \right\}, \tag{15}$$

which is promptly recognized as the standard-form of Tikhonov regularization, whose solution can be written as

$$\tilde{\mathbf{q}} = \tilde{\mathbf{G}}^H (\tilde{\mathbf{G}}\tilde{\mathbf{G}}^H + \eta^2 \mathbf{I})^{-1} \mathbf{p}, \tag{16}$$

where $\tilde{\mathbf{G}}$ is defined as $\tilde{\mathbf{G}} = \mathbf{G}\mathbf{W}^{-1}$. The singular value decomposition of the modified transfer matrix is written as:

$$\tilde{\mathbf{G}} = \mathbf{U} \lceil \mathbf{S} \rfloor \mathbf{V}^H \tag{17}$$

where $\mathbf{U}$ is the $M \times M$ matrix of left singular vectors of $\tilde{\mathbf{G}}$, $\lceil \mathbf{S} \rfloor$ the diagonal matrix of singular values of $\tilde{\mathbf{G}}$ and $\mathbf{V}$ is the $N \times N$ matrix of right singular vectors of $\tilde{\mathbf{G}}$. The solution of Eq. (16) is conveniently expressed in terms of the singular value decomposition of $\tilde{\mathbf{G}}$ (Eq. (17)) which yields:

$$\tilde{\mathbf{q}} = \mathbf{V} (\lceil \mathbf{S} \rfloor^2 + \eta^2 \mathbf{I})^{-1} \lceil \mathbf{S} \rfloor \mathbf{U}^H \mathbf{p}, \tag{18}$$

with η a unknown regularization parameter. The reconstructed source field is then simply given by the back transformation:

$$\hat{\mathbf{q}} = \mathbf{W}^{-1} \tilde{\mathbf{q}}. \tag{19}$$

The above idea may be implemented in an iterative manner, for instance, by defining a weighting matrix $\mathbf{W}$ depending on the equivalent source distribution estimated at a previous step, such that:

$$W_{ij}^{(n)} = \delta_{ij} \left| \hat{q}_i^{(n-1)} \right|^{-1}, \tag{20}$$

where δ_{ij} is the Kronecker delta and n is the index of the actual solution. The estimate of the equivalent source distribution is returned by iteratively solving an updated quadratic function at each iteration. The iteration process is stopped when a convergence criterion is met. This is done here by evaluating the difference between consecutive estimates of the equivalent source distribution such as:

$$\varepsilon = 10 \log \left(\left\langle \left| \hat{q}_i^{(n)} / \hat{q}_i^{(n-1)} \right| \right\rangle \right), \tag{21}$$

with the operator $\langle \bullet \rangle$ denoting a spatial average. The iteration process may be stopped, for instance, when ε is inferior to 0.1 dB. In practice, in order to avoid zero valued weight coefficients in Eq. (20), a truncation on $\hat{\mathbf{q}}^{(n-1)}$ is imposed at each iteration such that only those values

within a threshold of 100 dB below the maximum of $\hat{\mathbf{q}}^{(n-1)}$ are kept.

The estimation of an optimal regularization parameter η in Eq. (18) is a crucial step in order to achieve a good estimate of the reconstructed field. Several *ad hoc* techniques to perform this task, such as the L-curve [13], the Generalized Cross Validation (GCV) [9] or the Normalized Cumulative Periodgram (NCP) [12], have been applied in acoustics and vibration problems [4, 10, 15, 17]. The above techniques and a recent method derived from a Bayesian framework [1] are extensively evaluated in [22] by means of numerical and experimental validations in acoustics. The superiority of the Bayesian regularization criterion to acoustic inverse problems is demonstrated, this criterion being a robust alternative for this kind of problems. The Bayesian estimate of the regularization parameter is returned by the minimization of the following cost function:

$$\mathbf{J}(\eta^2) = \sum_{k=1}^{M} \ln\left(s_k^2 + \eta^2\right) + (M-2)\ln\left[\frac{1}{M}\left(\sum_{k=1}^{M} \frac{|y_k|^2}{s_k^2 + \eta^2}\right)\right], \tag{22}$$

where s_k is the k-th singular value as returned from the decomposition in Eq. (17) and y_k is the k-th element of vector

$$\mathbf{y} = \mathbf{U}^H \mathbf{p}, \tag{23}$$

where $\mathbf{U}$ is a matrix whose columns are the left singular vectors from the decomposition in Eq. (17). In practice, the minimization is done by defining a grid of potential values of η^2 and choosing the one which minimizes the cost function in Eq. (22).

2.4 Theoretical comparison

As seen in the previous sections, the GIB and the iESM algorithms are based on an iterative scheme which allows source reconstructions with an improved spatial resolution. Indeed, weighting the transfer matrix by the estimated amplitudes of equivalent sources of the previous iteration enhances the sparsity of the source distribution because only equivalent sources of high amplitudes remain in the end of the algorithm. It is the key principle of the Iteratively Reweighted Least Square algorithm [14] to compute sparse reconstruction.

The use of multipole transfer functions in the GIB algorithm is justified by the aeroacoustic environment of Suzuki's case study. Indeed, in an aeroacoustic measurements, most acoustic sources have a dipole radiation pattern, especially aeroacoustic sources associated with an interaction between a sharp end and a flow. Even though no condition prevents the integration of multipole transfer functions in the iESM algorithm, the requirement to build a method to quantify acoustic sources has motivated the use monopole transfer function volume velocity-pressure [22].

The last but not least difference is clearly the strategy of regularization. Indeed, in the Eq. (7) Suzuki recommends a resolution by the generalized inverse with the determination of the regularization parameter by a diagonal loading method [25]. The regularization imposed for the iterative ESM is based on the estimation of a regularization parameter which depends on how the measured data is coupled to the inverse problem. This is done here by the minimization of the cost function in Eq. (22) derived from a Bayesian formalism. Both methodologies have the same goal which is to improve the conditioning of the transfer matrix $\mathbf{G}$ to be inverted (see Eq. (4)). Another difference remains in the numerical computation of the solution at each

	GIB algorithm [25]	iESM algorithm [22]
1. Formulation of direct problem	$\mathbf{p}_m = \mathbf{G}\mathbf{q}_m$, where $\mathbf{p}_m$ is the m^{th} mode of Λ	$\mathbf{p} = \mathbf{G}\mathbf{q} + \mathbf{n}$, where $\mathbf{p}$ is a vector of complex acoustic pressure
2. Solution of the problem	L_p-norm minimization $\hat{\mathbf{q}}_m = \arg\min_{\mathbf{q}_m} \|\mathbf{p}_m - \mathbf{G}\mathbf{q}_m\|_2^2 + \eta^2 \|\mathbf{q}_m\|_p^p$ with $p = 1$	General-form Tikhonov regularization $\hat{\mathbf{q}} = \arg\min_{\mathbf{q}} \left\{ \|\mathbf{p} - \mathbf{G}\mathbf{q}\|_2^2 + \eta^2 \|\mathbf{W}\mathbf{q}\|_2^2 \right\}$ with $\mathbf{W}$ invertible and setting $\mathbf{q} = \mathbf{W}^{-1}\tilde{\mathbf{q}} \quad \tilde{\mathbf{G}} = \mathbf{G}\mathbf{W}^{-1} \quad \tilde{\mathbf{G}} \overset{\text{svd}}{=} \mathbf{U}\lceil\mathbf{S}\rfloor\mathbf{V}^H$
a. Estimated sources	$\hat{\mathbf{q}}_m^{(n)} = \mathbf{W}_m^{(n)}\mathbf{G}^H \left[\mathbf{G}\mathbf{W}_m^{(n)}\mathbf{G}^H + \eta^2\mathbf{I}\right]^{-1} \mathbf{p}_m$	$\tilde{\mathbf{q}} = \mathbf{V}(\lceil\mathbf{S}\rfloor^2 + \eta^2\mathbf{I})^{-1}\lceil\mathbf{S}\rfloor\mathbf{U}^H\mathbf{p}$ $\hat{\mathbf{q}}^{(n)} = \mathbf{W}^{-1}\tilde{\mathbf{q}}$
b. Weighting coefficients	$\forall (i,j) \in [1, N \times N_{type}]^2, \quad W_{ij,m}^{(n)} = \delta_{ij} \left\|\hat{q}_{i,m}^{(n-1)}\right\|$	$\forall (i,j) \in [1,N]^2, \quad W_{ij}^{(n)} = \delta_{ij} \left\|\hat{q}_i^{(n-1)}\right\|^{-1}$
c. Regularization parameter	$\eta^2 = 1\%$ of the greatest eigenvalue of $\mathbf{G}\mathbf{W}_m^{(n)}\mathbf{G}^H$	η^2 estimated from the data by minimization of cost function in Eq. (22)
d. Stopping criteria	Convergence criterion: $\|\hat{\mathbf{q}}_m^{(n)}\|_1 > \|\hat{\mathbf{q}}_m^{(n-1)}\|_1$ Underdetermined problems: $2M > \beta^n \times N \times N_{type}$	Convergence criterion: $\varepsilon = 10\log\left(\left\langle\left|\hat{q}_i^{(n)}/\hat{q}_i^{(n-1)}\right|\right\rangle\right) < 0.1\text{dB}$

Table 1: A schematic comparison of the GIB algorithm and the iESM algorithm

iteration. The iterative ESM is based on a singular value decomposition of a weighted transfer matrix, while the generalized inverse beamfoming computes a regularized pseudo-inverse of the transfer matrix. A schematic representation of both algorithms is presented in Table 1.

3 SIMULATIONS : BENCHMARK PROBLEMS

In this section, both methods are compared on benchmark configurations defined by Suzuki [25], these simulated test cases are presented in order to confirm the theoretical capability to identify complex source type such as: distributed sources, coherent sources and dipole sources. All spatial dimensions are normalized by the wavelength and all the speeds are normalized by the acoustic wave celerity c. To satisfy this normalization property, the choice was made not to normalize those parameters but to work at the frequency $f = 340Hz$ so that the wavenumber is equal to $k = 2\pi$ and the wavelength is equal to $\lambda = 1m$ with an acoustic celerity value of $c = 340m.s^{-1}$.

3.1 Problem geometries

The microphone array considered for these benchmark problems is an array of 60 microphones which are distributed on six arms corresponding to a portion of logarithmic spiral duplicated six times by rotation around the center of the array. The array is located on the z-axis at coordinates $z = 10m$, the origin of the cartesian coordinates is at the center of the equivalent source plane.

The microphone array geometry is represented by black circles in Fig. 1.
The calculation grid is a discretized plane whose points represent equivalent acoustic sources, it is a $6m \times 6m$ square grid with a grid spacing of $0.25m$ (625 calculation points). The calculation grid is represented by red circle in Fig. 1.

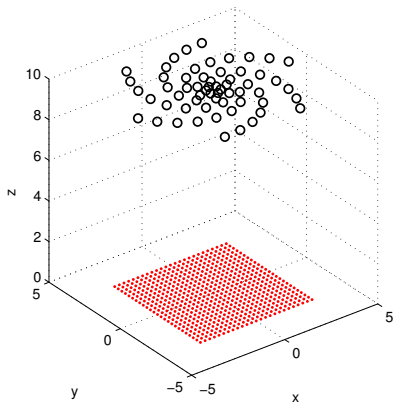

Figure 1: Diagram of the problem geometries: the microphone array geometry in black circle and the equivalent source plane in red circles.

3.2 Acoustic transfer functions

The acoustic transfer functions used for the computation of the results for the benchmark problems and the experiments are of three types: monopole pressure-volume velocity transfer functions, monopole pressure-pressure transfer functions and dipole pressure-pressure transfer functions. The iESM algorithm recovers equivalent sources of acoustic volume velocity from the pressure measured by the microphone array. Thus, the pressure-volume velocity transfer function [22] linking a source point $\mathbf{r}_n$ to a measuring point $\mathbf{r}_m$ is computed using the following expression:

$$g_{mono,vol}(\mathbf{r}_m \mid \mathbf{r}_n) = j\rho ck\frac{\exp\left(-jk\|\overrightarrow{r_n r_m}\|\right)}{4\pi\|\overrightarrow{r_n r_m}\|} \tag{24}$$

where the convention $-j$ is assumed in this study and ρ the density of the fluid. The reconstruction of equivalent sources of acoustic volume velocity is used for localization results in the following and also useful for the quantification. The transfer matrix $\mathbf{G}$ of the Eq. (18) is a set of monopole transfer functions $g_{mono,vol}$.

On the other hand, the GIB algorithm aims to reconstruct equivalent sources of acoustic pressure taking into account the eventual dipole directivity of the equivalent sources. Hence, the expression of the monopole pressure-pressure transfer function linking a source point $\mathbf{r}_n$ to a measuring point $\mathbf{r}_m$ is [25]:

$$g_{mono}(\mathbf{r}_m \mid \mathbf{r}_n) = \frac{\exp\left(-jk\|\overrightarrow{r_n r_m}\|\right)}{4\pi\|\overrightarrow{r_n r_m}\|} \tag{25}$$

and the dipole pressure-pressure transfer function linking a source point $\mathbf{r}_n$ to a measuring point

$\mathbf{r}_m$ characterizing a dipole point source making an angle θ with the x axis is [25]:

$$g_{dip}(\mathbf{r}_m \mid \mathbf{r}_n) = \overrightarrow{r_n r_m}.(cos\theta, sin\theta, 0)\frac{(-1+jk\|\overrightarrow{r_n r_m}\|)\exp(-jk\|\overrightarrow{r_n r_m}\|)}{2k\|\overrightarrow{r_n r_m}\|^3} \tag{26}$$

Noting $g_{dip,x}$ the transfer matrix associated with dipole oriented in the x direction ($\theta = 0°$) and $g_{dip,y}$ the transfer matrix associated with dipole oriented in the y direction ($\theta = 90°$), the transfer matrix $\mathbf{G}$ used in Eq. (7) contains transfer functions $g_{dip,x}$ as well as transfer functions $g_{dip,x}$ in order to allow the GIB algorithm to discriminate monopole and dipole equivalent sources.

Let $P_{GIB,x-dip}$ be the complex amplitude vector of the estimated dipole equivalent sources in the x direction and let $P_{GIB,y-dip}$ be the complex amplitude vector of the estimated dipole equivalent sources in the y direction. In section 3 and in section 4, the noise maps which are labeled "GIB dipole part" are superpositions of a pressure map whose levels are set to be $20\log_{10}\left(P^2_{GIB,x-dip}(\mathbf{r}_n)+P^2_{GIB,y-dip}(\mathbf{r}_n)\right), \forall n \in [1,N]$ and of green arrows. A green arrow at the location $\mathbf{r}_n$ makes an angle $\hat{\theta}(\mathbf{r}_n)$ with the x axis (Eq. (27)) and has a length equal to $10\log_{10}\left(P^2_{GIB,x-dip}(\mathbf{r}_n)+P^2_{GIB,y-dip}(\mathbf{r}_n)\right)$.

$$\hat{\theta}(\mathbf{r}_n) = \arctan\left(\frac{P_{GIB,y-dip}(\mathbf{r}_n)}{P_{GIB,x-dip}(\mathbf{r}_n)}\right) \tag{27}$$

Mathematically, $\hat{\theta}(\mathbf{r}_n) = 0°$ when $P_{GIB,x-dip}(\mathbf{r}_n) = 0$ which means that only an x-dipole exists at $\mathbf{r}_n$ and $\hat{\theta}(\mathbf{r}_n) = 90°$ when $P_{GIB,y-dip}(\mathbf{r}_n) = 0$ which means that only an y-dipole exists at $\mathbf{r}_n$. Furthermore, it has been verified that any simulated dipole sources with an orientation θ generates a green arrow with orientation $\hat{\theta} = \theta$ in the GIB estimate.

3.3 Localization results

The elementary case defined by Suzuki [25] of a single monopole was tested and validated the ability of the two methods to localize a point source with a great resolution. In the following, critical cases are examined in order to evaluate the limitations of each method. Two benchmark cases are considered: a coherent pair of a monopole and a dipole and a distributed source. For these test cases, only localization results are used for the comparison of both methods, consequently the acoustic quantities reconstructed are the real part of the volume velocity for the iESM and the pressure for the GIB using the acoustic transfer functions explicited in the previous subsection.

The first simulated case is the case of two coherent sources: a monopole source located at $(-1m, 0m, 0m)$ and a y-dipole source located at $(+1m, 0, 0)$ as represented by the red spots in the background of Fig. (2). The coherence between both sources is ensured by simulating them in phase. According to Fig. 2(a) and Fig. 2(b), both algorithms manage to localize the monopole source with a good resolution. Concerning the dipole source, the iESM algorithm reconstructing equivalent sources of acoustic volume velocity, the result is the juxtaposition of two point sources in phase opposition centered in the position of the dipole source (Fig. 2(a)). On the other hand, the GIB method recovers the localization and the orientation of the dipole source (green arrows in Fig. 2(c)) by taking into account dipole transfer functions in its inversion process. Thus, this test case highlights the theoretical capability of both algorithms

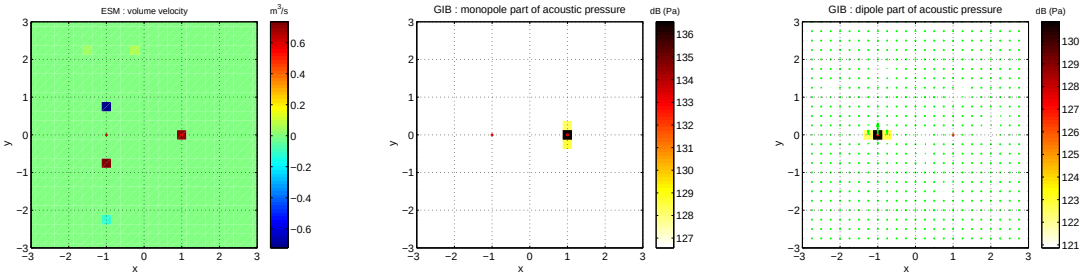

(a) iESM (b) GIB monopole part (c) GIB dipole part

Figure 2: Comparison of noise-source maps of a monopole source located at $(+1m, 0m, 0m)$ *and a y-dipole source located at* $(-1m, 0, 0)$ *which are both coherent.*

to identify dipole sources although in a complex environment the use of monopole equivalent source of volume velocity will be of limited interest because it splits point dipole sources into two point monopole sources. The monopole source and the dipole source are localized by both methods, which demonstrates the localization performance of the methods against source coherence. For this case, only one mode of the cross spectral matrix is energetic and the iESM computes its equivalent source distribution of in 12 iterations, whereas the GIB algorithm realized 27 iterations.

The second simulated case is the case of a distributed source modelled as a line of twelve coherent monopole sources with an inclination of 30° in the cartesian plane as represented by the red spots in the background of Fig. 3. Regarding Figs. 3(a) and 3(b), the two algorithms manage

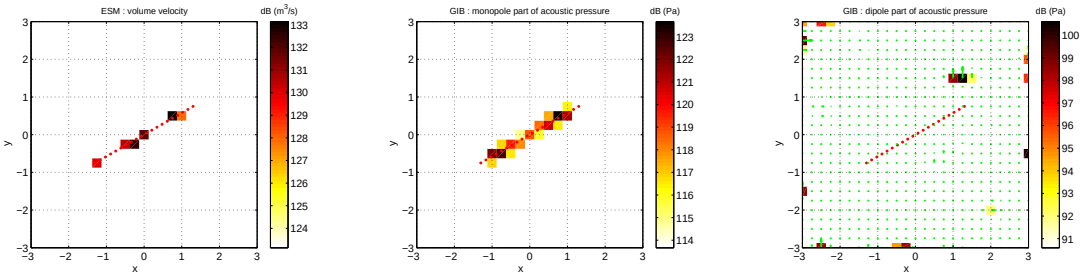

(a) iESM (b) GIB monopole part (c) GIB dipole part

Figure 3: Comparison of noise-source maps of a distributed source with an inclination of 30° *relative to the x direction.*

to localize the line source. However, it can be noted that both methods tend to enforce the spatial sparsity when reconstructing the distribution of equivalent sources because of the iterative structure of the algorithms and the weighting by the estimated amplitude of the equivalent sources calculated from the previous result. This is one of the limitation of the L_1-norm reconstruction algorithms because they provide no physical solution in presence of distributed sources. Fig. 3(c) shows that little energy is assigned to the dipole part of the equivalent sources during the processing of GIB, the amplitudes of the dipole part of the estimated equivalent sources are 20dB smaller than the amplitudes of the estimated equivalent sources of the monopole part.

In consequence the inverse algorithm using monopole transfer function and dipole function is able to distribute the energy according to the correct source type with a good dynamic range. Concerning computational efficiency, only one mode of the cross spectral matrix is energetic and the iESM computes its equivalent source distribution using 21 iterations, whereas the GIB algorithm realized 27 iterations. The GIB iterative process stops at 27 iterations because of the stopping criteria of Eq . (10), it justifies why the GIB result (Fig. (3(b))) is less sparse than the iESM result (Fig. (3(a))).

To conclude, those simulations consolidate the theoretical high performances of inverse methods for the localization of complex sources, the next section deals with their performances for the processing of measured data. Although the iESM seems to be limited in resolution for the localization of dipole sources, there is no restriction to implement the iESM algorithm using dipole transfer function. The enhancement of spatial resolution of the noise maps should not be performed regardless of the validity the assumption of a sparse source distribution, otherwise the algorithms will provide no physical results. Moreover, for every benchmark cases, the iESM method processes less iterations than the GIB which supports the hint in subsection 2.4 about the optimality of Tikhonov regularization for finding the regularization parameter at each iteration.

4 EXPERIMENTAL ILLUSTRATION

An experimental application of the Generalized inverse beam-forming and the iterative ESM in an academic aeroacoustic experiment is presented in this section. The experiment consists of an open-jet anechoic wind tunnel at the Ecole Centrale de Lyon (ECL). The airflow speed was measured by a pitot tube and is equal to 40 m/s for the experimental results shown here. Two side plates extending the nozzle are used in order to fix obstacles on the flow. A planar array of 54 pressure microphones is placed outside the flow at a distance of 34.5 cm and normal to the flow direction. A 6mm diameter rod is placed in between the two side plates, in the potential core of the rectangular jet.

A distribution of elementary sources is positioned on a plane parallel to the flow and passing through the rod. This fictitious source plane extends the side plates and has a dimension of 80 cm x 68 cm with a grid spacing of 2 cm. It is assumed that the propagation between elementary sources and the microphone array is in free-field, the effects introduced by the side plates (reflections, diffraction) are thus not taken into account in the model. A distribution of monopoles is used for the iterative ESM, while a distribution of monopoles and dipoles for the generalized inverse beam-forming. Acoustic imaging results are computed for a frequency band centered at 1400 Hz, which corresponds to a Strouhal number $Sr = f_0 d/U_\infty = 0.21$, where d is the rod diameter and U_∞ the free stream velocity.

The results for both methods are shown in Fig. 4. It can be seen that the iterative ESM identifies a source at the midspan of the rod and slightly stretched normally to the rod. The generalized inverse beam-forming returns a monopole contribution around 10 dB above the dipole contribution. The monopole part shows a reconstructed source slightly to the left of the rod and concentrated at its midspan. Dipole components are also identified at the midspan of the rod and oriented perpendicularly to the stream direction, towards the spanwise direction (see Fig. 4(c)).

Although one should normally expect sources distributed along the rod span, both methods

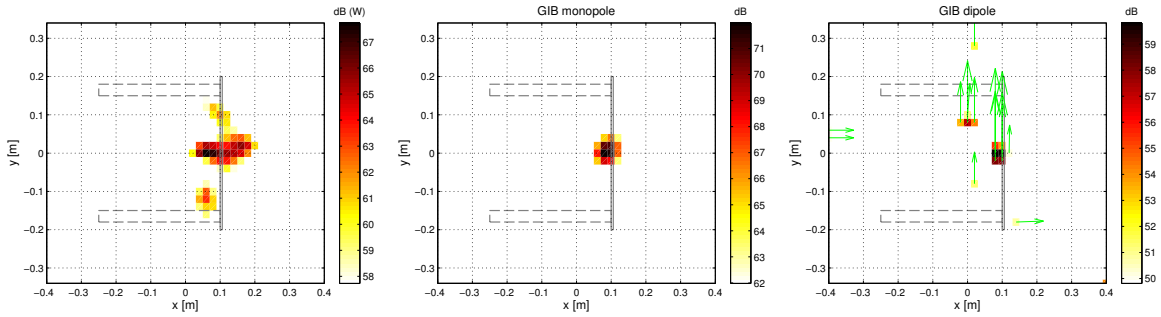

(a) iESM (b) GIB monopole part (c) GIB dipole part

Figure 4: Acoustic maps integrated over 1340 Hz to 1460 Hz. The two side plates and the rod are also sketched on the figures. The air flow direction is from left to right.

identify rather concentrated sources at midspan. The reason for this observation is still not very clear and requires further investigation. The confinement effect introduced by the side plates (such as reflections or diffraction of acoustic waves), may be a possible explanation, since they are not taken into account in the model. The above is currently being evaluated by means of numerical approaches such as FEM and BEM.

5 CONCLUSIONS

A comparison between two techniques dedicated to acoustic imaging has been presented in this paper. Despite being proposed for different application scenario, it is shown that they share a similar mathematical formulation. Generalized inverse beam-forming imposes a relatively severe regularization at each iteration, while the iterative ESM seeks an optimal data dependent regularization. Consequently, it is shown that the iterative ESM normally requires fewer iterations in order to compute localization results with reasonable spatial resolution. It is shown, however, that over iteration produces very sparse solutions which may be difficult to interpret in practice. The experimental characterization of the acoustic sources generated by a rod placed in an open jet wind tunnel has been presented in the last part. The results of both methods indicate sources located at the proximities of the rod, although concentrated at the midspan. The installation effects introduced by the side plates is currently being investigated in order to estimate its influence on the acoustical imaging results.

6 ACKNOWLEDGEMENTS

This work is financially supported by DGA/MRIS (*Direction Générale de l'Armement*). This work is also performed within the framework of the project SEMAFOR supported by the FRAE (Fondation de Recherche pour l'Aéronautique et l'Espace).

REFERENCES

[1] J. Antoni. "A bayesian approach to sound source reconstruction: Optimal basis, regularization, and focusing." *The Journal of the Acoustical Society of America*, 131(4), 2873–2890, 2012.

[2] T. F. Brooks and W. M. Humphreys, Jr. "A Deconvolution Approach for the Mapping of Acoustic Sources (DAMAS) Determined from Phased Microphone Arrays." AIAA-2004-2954, 2004. 10th AIAA/CEAS Aeroacoustics Conference, Manchester, Great Britain, May 10-12, 2004.

[3] G. Chardon, L. Daudet, A. Peillot, F. Ollivier, N. Bertin, and R. Gribonval. "Near-field acoustic holography using sparse regularization and compressive sampling principles." *The Journal of the Acoustical Society of America*, 132(3), 1521–1534, 2012.

[4] H. G. Choi, A. N. Thite, and D. J. Thompson. "Comparison of methods for parameter selection in tikhonov regularization with application to inverse force determination." *Journal of Sound and Vibration*, 304(3-5), 894 – 917, 2007. ISSN 0022-460X.

[5] N. Chu, A. Mohammad-Djafari, and J. Picheral. "Robust bayesian super-resolution approach via sparsity enforcing a priori for near-field aeroacoustic source imaging." *Journal of Sound and Vibration*, (0), 2013. ISSN 0022-460X.

[6] H. Cox, R. Zeskind, and M. Owen. "Robust adaptive beamforming." *IEEE Transactions on Acoustics, Speech and Signal Processing*, 35(10), 1365–1376, 1987.

[7] R. P. Dougherty. "Advanced Time-domain Beamforming Techniques." AIAA-2004-2955, 2004. 10th AIAA/CEAS Aeroacoustics Conference, Manchester, Great Britain, May 10-12, 2004.

[8] R. P. Dougherty. "Improved Generalized Inverse Beamforming for Jet Noise." AIAA-2011-2769, 2011. 17th AIAA/CEAS Aeroacoustics Conference (32nd AIAA Aeroacoustics Conference), Portland, Oregon, June 5-8, 2011.

[9] G. H. Golub, M. Heath, and G. Wahba. "Generalized cross-validation as a method for choosing a good ridge parameter." *Technometrics*, 21(2), 215–223, 1979.

[10] J. Gomes. "A study on regularization parameter choice in near-field acoustical holography." *The Journal of the Acoustical Society of America*, 123(5), 3385–3385, 2008.

[11] P. Hansen. *Rank-Deficient and Discrete Ill-Posed Problems*. Society for Industrial and Applied Mathematics, Philadephia, PA, 1998. ISBN 9780898719697.

[12] P. C. Hansen, M. E. Kilmer, and R. H. Kjeldsen. "Exploiting residual information in the parameter choice for discrete ill-posed problems." *BIT Numerical Mathematics*, 46, 41–59, 2006. ISSN 0006-3835.

[13] P. C. Hansen and D. P. O'Leary. "The use of the l-curve in the regularization of discrete ill-posed problems." *SIAM J. Sci. Comput.*, 14, 1487–1503, 1993. ISSN 1064-8275.

[14] P. Huber. *Robust Statistics*. New York: John Wiley and Sons, 1981.

[15] Y. Kim and P. A. Nelson. "Optimal regularisation for acoustic source reconstruction by inverse methods." *Journal of Sound and Vibration*, 275(3-5), 463 – 487, 2004. ISSN 0022-460X.

[16] G. H. Koopmann, L. Song, and J. B. Fahnline. "A method for computing acoustic fields based on the principle of wave superposition." *The Journal of the Acoustical Society of America*, 86(6), 2433–2438, 1989.

[17] Q. Leclere. "Acoustic imaging using under-determined inverse approaches: Frequency limitations and optimal regularization." *Journal of Sound and Vibration*, 321(3-5), 605 – 619, 2009. ISSN 0022-460X.

[18] J. Li, P. Stoica, and Z. Wang. "On robust capon beamforming and diagonal loading." In *Acoustics, Speech, and Signal Processing, 2003. Proceedings. (ICASSP '03). 2003 IEEE International Conference on*, volume 5, pages V–337–40 vol.5. 2003. ISSN 1520-6149. doi:10.1109/ICASSP.2003.1199947.

[19] M. B. S. Magalhaes and R. A. Tenenbaum. "Sound sources reconstruction techniques: A review of their evolution and new trends." *Acta Acustica united with Acustica*, 90(2), 199–220, 2004.

[20] J. D. Maynard, E. G. Williams, and Y. Lee. "Nearfield acoustic holography: I. Theory of generalized holography and development of NAH." *J. Acoust. Soc. Am.*, 78, 1395–1412, 1985.

[21] A. Peillot. *Imagerie acoustique par approximations parcimonieuses des sources*. Ph.D. thesis, Université Pierre et Marie Curie-Paris VI, 2012.

[22] A. Pereira. *Acoustic imaging in closed spaces*. Ph.D. thesis, INSA de Lyon, 2013.

[23] P. Sijtsma. "CLEAN based on spatial source coherence." *International Journal of Aeroacoustics*, 6, 357–374, 2007.

[24] T. Suzuki. "Generalized Inverse Beam-forming Algorithm Resolving Coherent/Incoherent, Distributed and Multipole Sources." AIAA-2008-2954, 2008.

[25] T. Suzuki. "L1 generalized inverse beam-forming algorithm resolving coherent/incoherent, distributed and multipole sources." *J. Sound Vib.*, 330, 5835–5851, 2011. doi:10.1016/j.jsv.2011.05.021.

[26] A. Tikhonov. "Solution of incorrectly formulated problems and the regularization method." In *Soviet Math. Dokl.*, volume 5, pages 1035–1038. 1963.

[27] P. A. G. Zavala, W. de Roeck, K. Hanssens, J. R. de Franca Arruda, P. Sas, and W. Desmet. "Generalized inverse beamforming investigation and hybrid estimation." BeBeC-2010-10, 2010. Proceedings on CD of the 3rd Berlin Beamforming Conference, 24-25 February, 2010.